Intercrystal Optical Crosstalk in Radiation Detectors: Monte Carlo Modeling and Experimental Validation

Carlotta Trigila, *Member, IEEE*, N. Kratochwil, *Member, IEEE*, B. Mehadji, G. Ariño-Estrada, *Member, IEEE*, and E. Roncali, *Senior Member, IEEE*

***Abstract*—High-performance radiation detectors often employ crystal arrays where light can leak between them, a phenomenon called intercrystal crosstalk, which demands mitigation for optimal detector performance. The complexity of measuring optical crosstalk in conventional detector geometries makes optical Monte Carlo simulation essential to study and reduce crosstalk through better designs. Addressing the absence of validated transmission models in Monte Carlo toolkits, we developed and integrated a new simulation model into the look-up table Davis Model, aiming at simulating optical photon refraction at the crystal interfaces using GATE. For the first time, we validated the intercrystal optical crosstalk model with experiments in two optically coupled Lutetium-yttrium oxyorthosilicate crystals read by two SiPMs, testing three thicknesses and four interfaces (air, glue, Teflon, and ESR). Simulated and experimental crosstalk agreed within one FWHM for all configurations. These results show the possibility of predicting optical photon transmission in detector designs with multiple crystal elements. Indeed, although validated using only two crystals, the model can be used in more complex geometries. The model, available to GATE users upon request, provides a valuable resource for researchers when optimizing detector geometry where optical crosstalk needs to be considered, i.e., ensuring optical isolation between the photodetector's responses.**

***Index Terms*—Crosstalk, crystal interfaces, intercrystal transmission, Monte Carlo simulation, optical coupling, TOF-PET.**

Manuscript received 7 February 2024; revised 26 March 2024, 19 April 2024, and 23 April 2024; accepted 26 April 2024. Date of publication 29 April 2024; date of current version 5 September 2024. This work was supported in part by the National Institutes of Health under Grant R01EB027130 and Grant R01 EB034062-01A1. *(Corresponding author: Carlotta Trigila.)*

This work did not involve human subjects or animals in its research.

Carlotta Trigila and N. Kratochwil are with the Department of Biomedical Engineering, University of California at Davis, Davis, CA 95616 USA (e-mail: ctrigila@ucdavis.edu).

B. Mehadji is with the Department of Radiology, University of California at Davis, Davis, CA 95616 USA.

G. Ariño-Estrada is with the Department of Biomedical Engineering, University of California at Davis, Davis, CA 95616 USA, and also with the Institut de Física d'Altes Energies-Barcelona Institute of Science and Technology, 08193 Barcelona, Spain.

E. Roncali is with the Department of Biomedical Engineering and the Department of Radiology, University of California at Davis, Davis, CA 95616 USA.

Color versions of one or more figures in this article are available at https://doi.org/10.1109/TRPMS.2024.3395131.

Digital Object Identifier 10.1109/TRPMS.2024.3395131

I. Introduction

NUCLEAR medicine systems involve using the scintillation detector crystals optically isolated from each other, packed in the crystal arrays. In such designs, the detector's performance can be substantially influenced by the intercrystal crosstalk, which could result from the Compton scattering (Compton crosstalk) or imperfect optical isolation (optical photon intercrystal crosstalk). This issue becomes more severe as crystals become thicker and narrower to enhance the spatial resolution [1], [2], [3], [4].

Compton crosstalk leads to systematic errors in the scintillation detectors with limited energy resolution because the pulse height discrimination stages cannot discriminate between the photoelectric and Compton interactions. As a result, a systematic positive count rate offset can result from the erroneously counted scattered photons. Gamma ray interaction in matter is well understood and modeled in commonly used simulation toolkits, and numerous studies have already investigated Compton crosstalk and its impact on the radiation detectors [1], [5], [6], [7]. The other type of crosstalk, the optical crosstalk between the crystals can negatively impact timing resolution, energy resolution, and positioning accuracy. Addressing intercrystal crosstalk in a high-resolution PET detector array could enhance image contrast, particularly in scenarios where crosstalk significantly contributes to the mispositioned events. The investigation of intercrystal optical photon crosstalk is thus of great interest and still under the investigation [8], [9], particularly in new detector configurations where optimal surface treatment and interfaces are investigated. However, it still needs to be accurately modeled and thoroughly investigated. In this context, optical Monte Carlo simulations are fundamental to modeling and studying the behavior of optical photons.

In this work, we focused on the intercrystal optical photon crosstalk and studied their effect on the overall detection of optical photons. First, we performed optical Monte Carlo simulations using the simulator GATE, a toolkit dedicated to numerical simulations in medical imaging and radiotherapy [11]. Optical photon reflections and transmissions through the interfaces were modeled using the look-up table (LUT) Davis model [12]. The model is based on an accurate 3-D representation of the crystal surface and has already been validated when simulating the reflection of optical photons

within a crystal [13]. It has been proven to be crucial for precisely modeling and understanding the transport of optical photons within a scintillator. The model enables accurate optical simulations to design and optimize scintillation detectors, especially when exploring various surface treatments, interfaces, and reflectors to assess their impact on nuclear medicine detector performances [14].

Here, the LUT model underwent optimization to include the angular distribution of optical photons as they refract through one or several interfaces. This enhancement encompassed the capability to simulate transmission through a reflector by integrating one or multiple reflections or refractions within the crystal-reflector coupling interface. The inclusion of transmission into the LUT altered their format, prompting a modification in the way GATE reads and manages the LUT. This adaptation enabled validation and comparison with experimental measurements. As the new LUTs are built by simulating photon transport in complex interfaces, careful experimental validation was required yet challenging due to the difficulty of separating optical crosstalk photons from the "primary" photons when collecting light with a photodetector.

The optical photon crosstalk was estimated in two optically coupled cerium-doped Lutetium-yttrium oxyorthosilicate (LYSO) crystals read out by two SiPMs, one at the top and one at the bottom of the crystals, both by simulation and experimental measurements. The detector design was optimized to optically decouple the two photodetectors' responses, allowing the experimental estimate of the optical crosstalk. Different crystal thicknesses (5, 10, and 20 mm) were used, and several crystal-crystal and crystal-reflector interfaces were tested. Air and Meltmount used to enhance the transmission between the two crystals, and ESR and Teflon used to mitigate the crosstalk. They allowed us to cover a range of crosstalk to validate the simulation.

II. Material and Method

A. Monte Carlo Simulations

Optical simulations were performed in two LYSO crystals to replicate the experimental setup, presented in the next section.

1) Detector Setup: Simulations were done using the open-source software GATE v. 9.2 (Geant4 v. 11) [11]. LYSO scintillation properties were defined as an isotropic emission following a single exponential decay with a time constant of 36 ns, a light yield of 33 000 ph/MeV, an emission spectrum with a peak at 420 nm, and an index of refraction varying between 1.85 and 1.79 between 370 and 800 nm. The absorption length was modeled in the same spectral range (from 0.72 to 190 mm in the 370–400 nm range, and 10 m from 400 to 800 nm [15]). Simulations were conducted using a 511 keV monoenergetic source located at 10 cm from the center of two laterally coupled LYSO crystals (crystals 1 and 2), perpendicular to their lateral faces [Fig. 1(a)] to guarantee the crystal's symmetric irradiation. 5, 10, and 20 mm thick LYSO crystals were tested, all with a 3×3 mm^2 cross section. Two $3 \times 3 \times 0.1$ mm^3 photodetectors were placed at the bottom and top surface of the first and second crystal, respectively, [photodetectors 1 and 2 in Fig. 1(a)]. While unconventional compared to the typical setup of utilizing two SiPMs on a single side of the crystal, employing a pair of photodetectors positioned beneath and atop the crystals proved to be the most effective in optically isolating the responses of the two SiPMs, thereby preventing any light leakage at the interface between the crystal and the photodetectors. The photodetectors were optically coupled with the crystals using a 15 μm-thick coupling material (Cargille Meltmount, index of refraction of 1.58). This value was estimated in the experimental setup using a caliper, which gave a Meltmount thickness in the range 0.01–0.02 mm. Both photodetectors had a Silicone protection window (n = 1.57 [16]) and were considered ideal, with a photon detection efficiency of 1, including geometrical and quantum efficiencies. A total of 5×10^5 gamma photons were emitted per simulation, both the photoelectric and Compton interactions with the crystals were considered, using the LYSO properties. The optical photons produced by scintillation and Cerenkov emission from energetic electrons were simultaneously generated and tracked using an electromagnetic physics list in Geant4 (*emstandard_opt4*), optimized for the low-energy models.

2) Detector Interfaces: The behavior of optical photons at the crystal edges was simulated using the LUT Davis model. The LUT Davis algorithm computes the reflection and refraction probabilities and the photons' angular distributions as a function of incidence angles (from 0° to 90°) of 3-D crystal surfaces scanned with atomic force microscopy, coupled to a reflector through a coupling medium (Fig. 2). The crystal is defined through its optical properties (emission spectrum and index of refraction (n_i) as a function of the wavelength). The coupling media is defined by its index of refraction (n_t) and thickness, while the absorption is not modeled. The reflector is modeled by its optical properties (reflectance and angular distribution of reflectance).

The first version of the LUT model has already been integrated into GATE, and several LUTs are available in the GATE database [12], [13]. However, only the reflection of optical photons was validated [13] (using the characteristics of the reflected photons, red arrows in Fig. 2). The transmission and the angular distribution of optical photons after refraction from the crystal to the coupling medium and from the reflector to the surrounding environment were not optimized nor validated.

In this work, the LUT Davis model algorithm was optimized to perform optical photon transmission modeling (blue arrows two in Fig. 2). Whenever an optical photon underwent refraction on the crystal surface, refraction followed by one or multiple reflections, or refractions within the multilayer crystal-reflector interface, its polar and azimuthal angles of refraction were computed using the index of refraction of the coupling medium and of the surrounding environment (n_e in Fig. 2, custom choice of the user, e.g., Air or LYSO). For the first time, multiple reflections in the crystal-reflector multilayer interface, followed by transmission in the environment, were included in the model.

The final LUTs included the reflectance and angles of reflection (already validated [13]) together with the transmittance

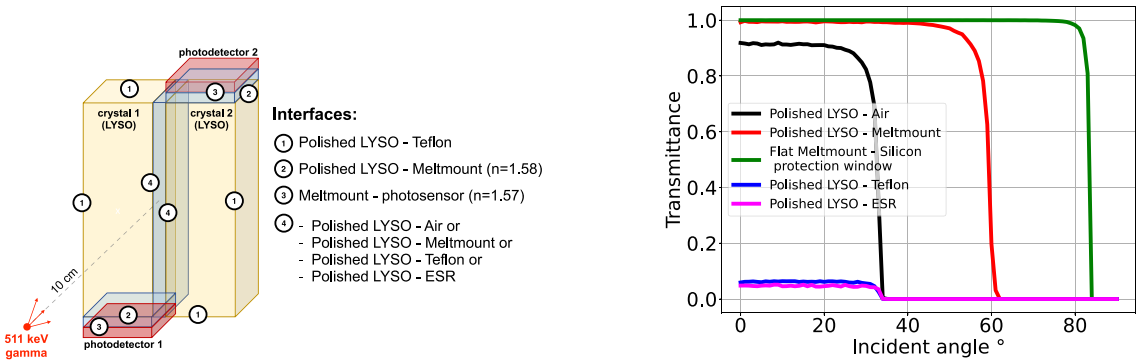

Fig. 1. (a) Simulation setup. Simulations were performed in two LYSO crystals. Several thicknesses were tested. We used two photodetectors, one at the top and one at the bottom of the crystals. Although different from the conventional approach of utilizing two SiPMs on the same side of the crystal, this configuration was optimal for optically decoupling the responses of the two SiPMs. Consequently, it mitigated any potential light leakage at the interface between the crystal and the photodetectors. Crystal interfaces with the surrounding environment were changed and customized using the LUT Davis model [10]. Volumes not to scale. (b) Transmittance of the generated customized LUTs as a function of the angle of incidence of the optical photons with respect to the normal of the surface.

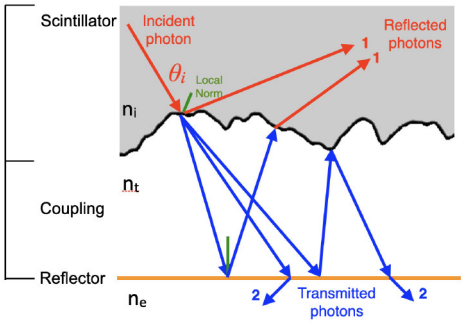

Fig. 2. Schematic view of the Davis LUT algorithm. The reflectance and transmittance LUTs for the scintillator–coupling medium interface are computed using 3-D crystal surface measurements, the scintillator intrinsic properties (emission spectrum and index of refraction (n_i) as a function of the wavelength) and the coupling medium index of refraction (n_t). If needed, the reflector LUT computation is performed using the reflector reflectivity and specific angular distribution of reflected photons. The reflectance of the optical photons was already validated [13] (reflected photons, red arrows one). In this work, we validate the modeling of the transmitted photons (blue arrows two) from the crystal surface and from the reflector to the environment (n_e, e.g., Air or crystal).

and a very detailed list of the angle of refraction (validated with this work). The absorption within the coupling medium was not included, but the optical photons performing more than 50 reflections within the interface (rare events, <0.1%) were removed. This allowed the incorporation of emission direction information following transmission into the LUT. This slightly modified the LUT structure, leading to adjustments in the GATE source code to interpret these LUTs properly.

Several customized interfaces [10] were generated using the optimized algorithm.

All crystal surfaces were polished and, except those between the two crystals and those in contact with the photodetectors, were wrapped in four layers of Teflon [interface 1, Fig. 1(a)]. To model the crystal coupling with the photodetector, a polished LYSO surface coupled with Meltmount was first used [interface 2, Fig. 1(a)]. Then, to simulate the coupling-photodetector interface, a perfectly flat surface between the Meltmount and the silicon protection window was used to generate the LUT [interface 3, Fig. 1(a)].

The two LYSO were optically coupled between each other in a sandwich configuration [interface 4, Fig. 1(a)], and four different coupling interfaces were tested: 1) air; 2) Meltmount; 3) ESR coupled with air; and 4) four layers-Teflon. Fig. 1(b) shows the different surface transmittance curves obtained after the LUTs generation.

GATE source code was finally modified to read these customized LUTs.

3) Data Processing and Analysis: The properties of all particles interacting within the crystal volumes and the information of the optical photons entering and exiting each interface were saved and analyzed using the Python.

To study the intercrystal optical crosstalk between the crystals 1 and 2 for all configurations, we grouped the optical photons detected on the photodetectors 1 or 2 and identified their emission position in crystals 1 or 2 and emission process (photoelectric or Compton gamma interaction) for each gamma interaction. For each gamma event, we extracted the number of detected optical photons on photodetectors 1 and 2, N_1 and N_2, respectively. We studied their distributions and the distribution of their sum N ($N = N_1 + N_2$) (Fig. 3). N_1 (or N_2) contained the events emitted in the crystals 1 or 2 but then detected by the photodetector 1 (or by photodetector 2). N contained the number of photons detected per gamma event and represented the overall energy distribution in the two crystals.

After selecting the events in the photopeak (within one FWHM), the ratio r was calculated for each event using

$$r = \frac{N_1}{N_1 + N_2}. \tag{1}$$

Two peaks characterized the distribution of r. The first peak represented the percentage of optical photons detected by the photodetector 1 that performed transmission after being emitted in crystal 2, while the second peak represented the percentage of photons emitted and detected by the crystal

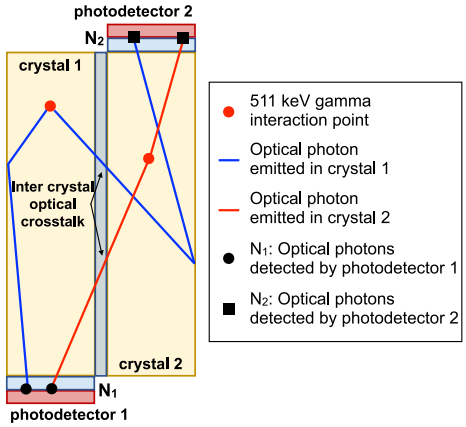

Fig. 3. Gamma and optical photons events organization. Dimensions not to scale.

1 (higher ratio, as expected). To account for the system symmetry, the fraction of optical crosstalk (CT) was finally calculated using

$$\mathrm{CT} = \frac{r_1 + (1 - r_2)}{2} \tag{2}$$

where r_1 and r_2 represented the mean positions of peaks 1 and 2, respectively. The uncertainty of CT was defined as the rms FWHM_1 and FWHM_2 obtained from the Gaussian fits of the two peaks characterizing the distribution of r

$$\mathrm{CT\ uncertainty} = \frac{\sqrt{\mathrm{FWHM}_1^2 + \mathrm{FWHM}_2^2}}{2}. \tag{3}$$

B. Experimental Setup

The experimental configuration is the same as in Fig. 1(a).

1) Detector Preparation: To prepare the sandwich detector, the interface between the two crystals was first assembled [Fig. 4(a)] either by putting the two unwrapped crystals in contact (air coupling), using Meltmount to glue the lateral side together, using four layers of 75 μm thick Teflon between the interface, or placing a thin ESR foil with dimensions matching the crystal face between the two bare crystals (3×5, 3×10, or 3×20 mm^2 depending on the LYSO thickness). Then, the two crystals were wrapped in Teflon along the lateral side [Fig. 4(b)] as well as the nonreadout crystal end [interface 1 as depicted in Fig. 1(a)] to provide mechanical stability and to avoid light leakage from the crystal 1 to photodetector 2 and vice versa. Crystal surfaces were all polished.

S14160 SiPMs from Hamamatsu Photonics (HPK, Hamamatsu, Japan), with 3×3 mm^2 active area and 50 μm microcell pitch, and silicon protection window (n = 1.57) were glued with Meltmount (n = 1.582) to the remaining crystal ends Fig. 4(c). To minimize correlated noise and SiPM crosstalk [17] as well as minimize SiPM saturation, the SiPMs were biased at a low overvoltage of about 2 V above breakdown voltage (V_{bias} = 40 V). A measurement of the SiPM crosstalk will be presented in the results.

Two radioactive sources (^{22}Na and ^{137}Cs) were used to generate gamma rays with respective energies of 511, 662, and 1.275 MeV for the saturation correction.

2) Data Processing and Analysis: SiPM signals were amplified with custom electronics based on an operational amplifier (AD8000). The waveforms were digitized with a DRS4 evaluation board from Paul Scherrer Institute (PSI, Villigen, Switzerland). An OR trigger was used. The trigger threshold for both the detectors was set at approximately 100 keV. The amplitude of the waveforms was used for energy selection and to derive the number of detected photons in each photodetector. SiPM saturation correction and energy calibration were performed individually for each configuration and photodetector following the procedure outlined in [18] to account for slight misalignment between the crystals end and photodetectors. Only events with full 511 keV energy deposition in one of the two crystals were considered in the analysis. Two distinct peaks always remain in the histogram.

1) The nontransmitted photons for interaction in the same crystal (photopeak).
2) The transmitted photons for interactions in the neighboring crystal (transmitted photopeak).

The experimental ratio of transmitted photons was calculated using

$$r = \frac{E_1}{E_1 + E_2} \tag{4}$$

where E_1 represents the energy distribution of the photodetector 1 and $E_1 + E_2$ the sum of the energy detected by the two photodetectors per gamma event. As for the simulation, the distribution of the experimental r is characterized by two peaks, which allowed us to extract the experimental percentage of optical crosstalk CT using the peak's mean values position using (2).

The comparison between CT from simulation and experiments permitted the validation of the transmission model integrated into the optical Monte Carlo simulations and to better understand the intercrystal optical crosstalk.

III. Result

A. Simulation Result

When a 511 keV gamma photon interacted in crystal 1, a part of the optical photons was detected by the photodetector 1, while the remainder was transmitted at the interface of the two crystals and detected by crystal 2 (Fig. 3).

Fig. 5 shows a spectrum representative of two 5 mm thick LYSO coupled with Meltmount. Among all events detected by the photodetector 1 [black curve in Fig. 5(a)], only events emitted and detected in crystal 1 [blue curve in Fig. 5(a)] contributed to the photopeak (centered on 7700 photons per gamma) and to the Compton shoulder (76% of events). Events emitted in crystal 2 and detected by the neighbor crystal 1 [red curve in Fig. 5(a)] contributed to the composition of the second peak (located at 2400 photons per gamma) and its Compton shoulder, and represented the transmitted events. The same spectrum was obtained with the events detected by the photodetector 2 [Fig. 5(b)] since the geometry is symmetric with respect to the source emission. The transmitted events were composed of the refracted optical photons emitted by both the photoelectric (13%) or Compton (12%) gamma

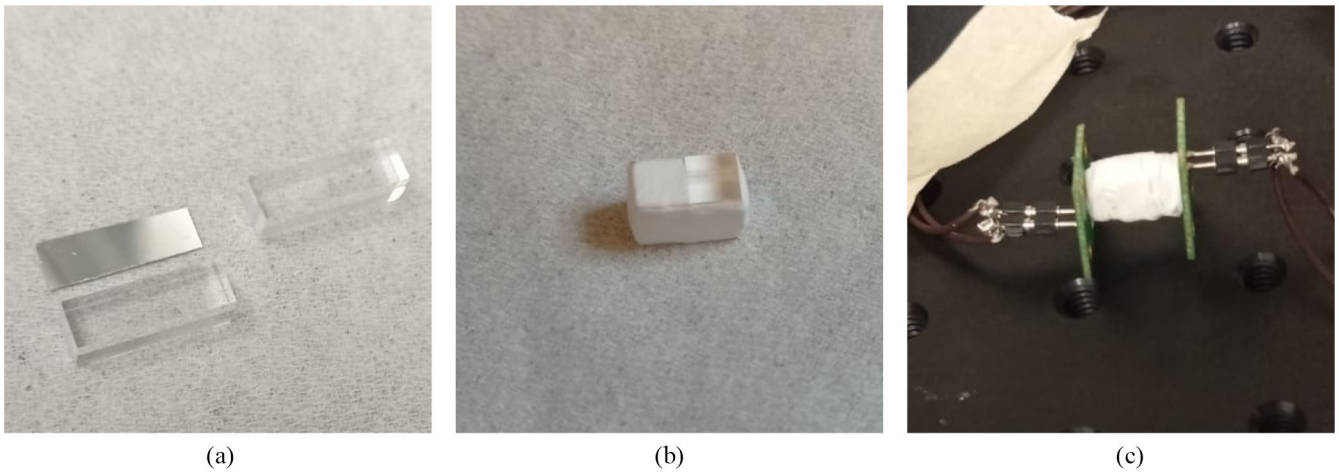

(a) (b) (c)

Fig. 4. Representative photos of the experimental setup with two polished $3 \times 3 \times 10$ mm^3 LYSO crystals. (a) LYSO crystals with ESR film to be placed between the lateral sides. (b) Top view of the crystals covered with Teflon, except one 3×3 mm^2 face that is supposed to be coupled with the SiPMs. (c) Wrapped crystals coupled to the SiPMs and readout board. Cables connected to custom electronics based on an operational amplifier (AD8000).

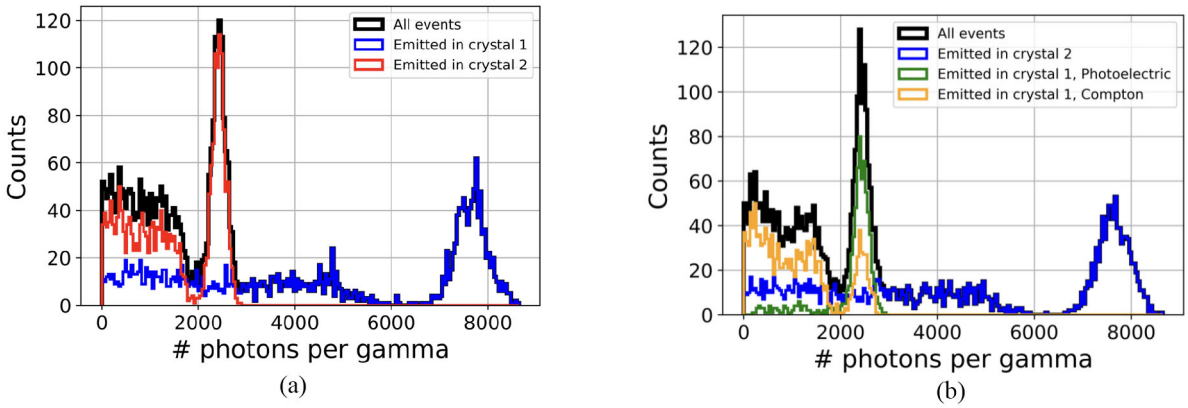

Fig. 5. (a) Simulated distribution of optical photons detected by the photodetector 1, N_1, per gamma event for a representative configuration (two 5 mm-thick LYSO coupled with Meltmount). Among all events (black), some were emitted in crystal 1 and detected in the same crystal (blue), while the remainder (red) were emitted in crystal 2 and performed a transmission at the interface of the crystal to be detected by the photodetector 1. (b) Simulated distribution of optical photons detected by the photodetector 2, N_2. The two spectra are equally shaped since the detector geometry is symmetrical with respect to the source emission position [Fig. 1(a)]. The transmitted events were decomposed according to the gamma interaction process that generated them: photoelectric (green) or Compton (yellow) event in crystal 2. In both spectra, after around 2400 detected photons per gamma, the black and blue curves superimpose, meaning that all the events contributing to the photopeak and beginning of the Compton shoulder were detected in the same crystal they were emitted.

interactions in crystal 1 [green and yellow curves, respectively, in Fig. 5(b)].

The distribution of the sum of the optical photons detected by both the photodetectors per gamma event N was a typical energy spectrum with a photopeak (10 000 photons per gamma) and a Compton shoulder and plateau [Fig. 6(a)], showing the complete photoelectric absorption of the gamma rays by the two detectors, net of any light absorption and transmission to the surrounding environment. Only the events in one FWHM of the photopeak were considered for the transmission calculation.

Using these events, the ratio between the optical photons detected by the photodetector 1 N_1 and the sum of the optical photons detected by both the photodetectors per events N gave the two peaks distribution shown in Fig. 6(b). The right peak (greater ratio) contains the optical photons detected by the photodetector 1 after a gamma ray interaction in crystal 1 and represents the detection of optical photons without transmission. The left peak contains optical photons detected by the photodetector 1 after a gamma ray interaction in crystal 2 and represents the transmitted photons from crystals 2 to 1. Two single Gaussian fits on these peaks allowed us to estimate the percentage of intercrystal optical crosstalk CT from simulation.

When using two 5 mm thick LYSO crystals coupled through Meltmount, around 24.2%±1.4% of all the optical photons detected by one photodetector performed an intercrystal optical transmission before detection (red Gaussian fit in Fig. 6(b), results are symmetric for both the photodetectors), while 75.9%±1.4% were detected by the same crystal, obtaining an intercrystal optical crosstalk of 24.2%±2.0% for this configuration. Uncertainty values for r_1, r_2 correspond to half the FWHM and the CT uncertainty was obtained from (3).

The same procedure was applied to all simulated configurations to extract the intercrystal optical crosstalk percentages.

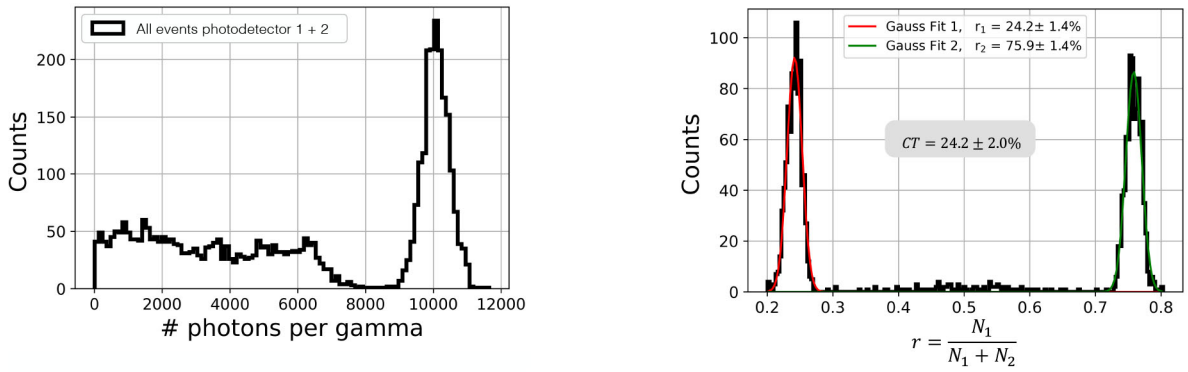

(a) (b)

Fig. 6. (a) Simulated overall spectra, given by the sum of all optical photons detected by the photodetectors 1 and 2 per gamma event N ($3 \times 3 \times 5$ mm^3 thick LYSO crystals coupled with Meltmount). (b) Simulated ratio between the photons detected by the first photodetector and the sum of all the optical detected by both photodetectors. The peak on the left represents the optical events performing intercrystal optical crosstalk, while the one on the right depicts the percentage of optical photons detected by the same photodetector after a gamma interaction. Two Gaussian fits of the peaks allowed extracting the percentage of intercrystal optical crosstalk from the simulation, CT. r_1 and r_2 uncertainties are defined by half the FWHM of a Gaussian fit applied to each peak. The CT uncertainty is the RMS value obtained from r_1 and r_2 (3).

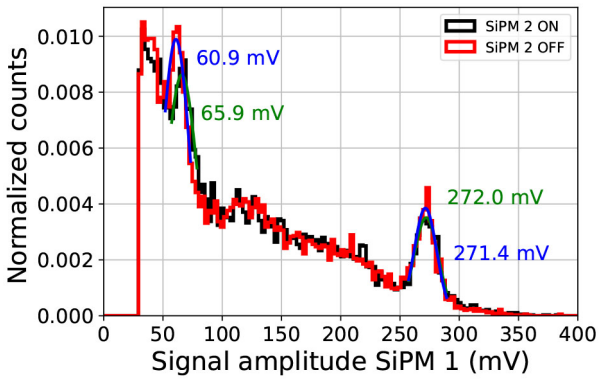

Fig. 7. SiPM 1 signal amplitude (without saturation correction or energy calibration), with the SiPMs biased or not. The SiPM bias voltage was 44 V (+6 V above breakdown voltage). Results after a ^{137}Cs irradiation. The position of the transmitted photopeak was shifted when the other SiPM was biased, likely due to SiPM crosstalk.

B. Experimental Result

1) Investigation of SiPM Crosstalk: The experimental measurements were conducted at the low SiPM overvoltage to minimize noise contributions from the SiPM crosstalk (bias voltage was 44 V and +6 V above breakdown voltage). To verify it, we conducted measurements with the second SiPM biased or unbiased. We used ^{137}Cs as source.

The peak position originating from the transmitted photons from the gamma ray interactions in crystal 2 was about 8% higher when the second SiPM was biased (Fig. 7, peak mean position shifted from 60.9 to 65.9 mV). The 622 keV photopeak (around 270 mV), which contains interactions in crystal 1, was not significantly changed. Performing the same measurement at +4 V led to $\approx$ 3% change of the transmitted peak position, while for +2 V overvoltage, no shift was observed. This led to the conclusion that the SiPM crosstalk probability was very low with a +2 V overvoltage, which was used throughout the presented work.

2) Experimental Intercrystal Optical Crosstalk: The 2-D distribution of the number of detected photons in SiPMs 1 and 2, after the SiPM saturation correction and energy calibration, showed a linear relationship between the number of detected optical photons from the SiPMs 1 and 2, indicated of the setup symmetry [Fig. 8(a)]. The calibration was performed so that 511 keV calibrated photons were assigned to events with a full 511 keV gamma ray energy deposition in the respective crystal and detected by the parent SiPM (ignoring the transmitted photons). Events between the main lines arose from energy deposition in both the crystals (Compton interaction and follow-up photoabsorption, and transfer of the hot recoil-electron to the neighboring crystal) and were discarded in the event selection.

The histogram of the number of detected photons for the individual SiPM shows a complex spectrum with different peaks [Fig. 8(b)], arising from either direct gamma ray interaction in the parent crystal or from transmitted photons from the neighboring crystal. For all tested configurations, the ratio of the transmitted and nontransmitted photons was calculated upon energy selection and following the same procedure described in the simulation section. When considering two 5 mm thick LYSO crystals coupled through Meltmount, around 30.7%±1.9% of the optical photons detected by one SiPM performed a transmission before being detected by the neighbor crystal (red Gaussian fit in Fig. 9). In contrast, 71.5%±1.9% were detected by the same crystal. This led to an experimental intercrystal optical crosstalk of 29.6%±2.7% for this configuration. The value obtained was in agreement with the simulated one (24.2%±2.0%). Uncertainties for r_1 and r_2 correspond to half the FWHM and the CT uncertainty is given by (3).

The same procedure was applied to all the configurations.

C. Simulation and Experimental Intercrystal Optical Crosstalk Comparison

The experimental and simulated intercrystal optical crosstalk showed good agreement for all configurations within one FWHM (Fig. 10). Independent from the thickness, the

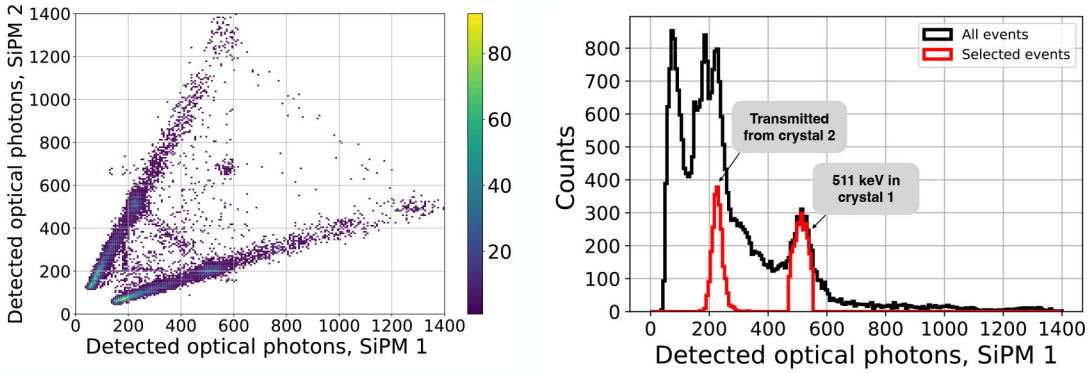

(a) (b)

Fig. 8. (a) Experimental 2-D histogram of the calibrated number of detected optical photons upon ^{22}Na excitation ($3 \times 3 \times 5$ mm^3 thick LYSO crystals coupled with Meltmount). (b) Experimental histogram of the calibrated number of detected optical photons in SiPM 1, without (black) and with (red) selection on the photopeak. The 511-keV photopeak (gamma ray interaction in crystal 1) and the corresponding peak from interactions in crystal 2 and light transmitted to crystal 1 are well visible. The spectrum of the detected optical photons by the SiPM 2 had a similar shape (not shown).

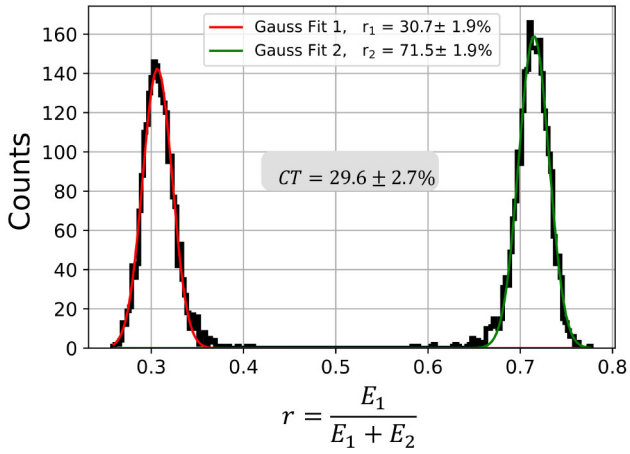

Fig. 9. Calculated ratio of detected photons for 5 mm-thick LYSO crystals coupled with Meltmount.

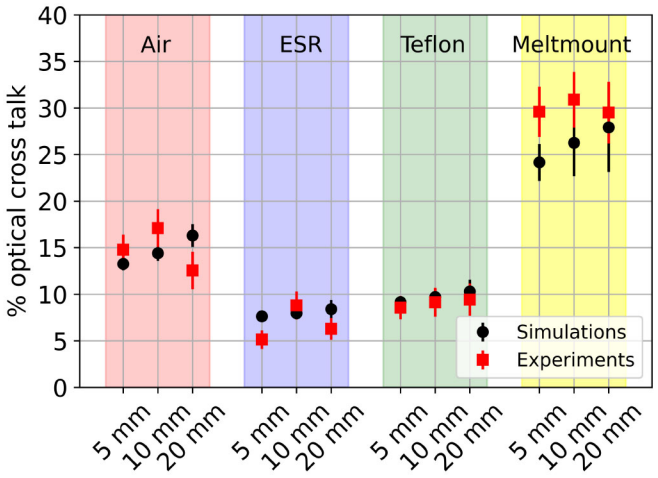

Fig. 10. Simulation and experimental intercrystal optical crosstalk (%) as a function of crystal thickness for all the configurations studied. The uncertainty of CT was defined as the RMS of the FWHM uncertainties obtained from the Gaussian fits depicted in Fig. 6(b), using (3).

fraction of optical crosstalk obtained with the four coupling materials tested reflected the transmittance trend shown in Fig. 1(b). The lowest optical crosstalk fractions were obtained using the ESR as coupling medium between the two crystals (lower than 8.5% for all thicknesses), which indeed appears to be the interface with the lowest transmittance for all incident angles [magenta curve, Fig. 1(b)]. The crosstalk slightly increased when using Teflon, reflecting the small difference in transmittance. With air, the transmission was favored with incident angles lower than ~32°, which was reflected by increased CT values (twice those of ESR for all thicknesses). The highest values were achieved with Meltmount (higher than 24% for all thicknesses), where almost all events arriving at the interface with an incident angle lower than 60° were transmitted. This result was expected since coupling the two crystals with a high-index material will decrease the index mismatch and thus increase transmission. However, the large differences in transmittance visible in Fig. 1(b) among some media (e.g., air and ESR, and Meltmount and ESR) did not reflect an equally large difference in CT. For example, an average transmittance that goes from 5% to 92% in the angular range between the 0° and ~32°, for ESR and air, respectively, (Fig. 1(b)), reflects only an average ~50% decrease in CT (Fig. 10). This was because a high probability of transmission [higher than 92%, like the one of air and Meltmount, Fig. 1(b)] favored the refraction from the crystal of emission to the neighbor but also the refraction back to the originating crystal. As a net effect, this reduced the CT to values lower than 20% and 30% for air and Meltmount, respectively.

For all configurations, the crosstalk increased as a function of the crystal thickness, as expected from a greater fraction of photons arriving at the two crystals' interface with the angles lower than the critical angles. Exceptions were obtained through experiments using the 20-mm thick crystals coupled with air, ESR, and Meltmount. This could be due to a sub-optimal optical coupling close to the SiPMs when using these materials because the experimental crystal wrapping close to the crystals interfaces at the photodetector faces was not trivial

(coupling between the crystals and the edges wrapping, made of Teflon). This suboptimal coupling, which could also be worsened by a nonperfectly rectangular shape of a crystal sample photodetector interface, could have led to the optical photon loss close to the photodetectors. This was not modeled in this work but has been documented [14]. Additionally, the FWHM increased with thicker crystals because the uncertainty of the calculated ratios increased due to light attenuation, spread, and poorer energy resolution.

IV. Discussion

We developed and validated a model for simulating the refraction of optical photons at the crystal interfaces, comparing it against experiments conducted on two coupled LYSO crystals with varying thicknesses. We tested four distinct coupling scenarios between the crystals: 1) air; 2) Meltmount; 3) ESR coupled with air; and 4) four layers of Teflon. The simulations exhibited a high level of agreement with the experimental results across all configurations. The results showed a small increase in crosstalk with varying crystal thicknesses, which remains low compared to the associated uncertainty when considering the same interface. Furthermore, they demonstrated that employing ESR resulted in the intercrystal optical crosstalk below 9%, whereas Meltmount exhibited values exceeding 24%. These values are representative of the coupling through a single interface and cannot be directly transferred to a complete crystal array. However, the validated model can be used to characterize the optical photon crosstalk of specific and more complex geometries.

The results show the critical role of selecting the crystal interface in mitigating crosstalk. Although not commonly used materials to couple crystals in arrays, air and Meltmount were used to favor refraction between the crystals, thus increasing the crosstalk for validation. ESR and Teflon were used as commonly used reflector materials, and both showed to be good candidates for reducing the CT. We did not test ESR coupled with grease since a loss of reflectivity of the ESR film coupled with grease was already reported [19], and this investigation was out of the scope of this work.

The presented model allows researchers to simulate optical photon refraction comprehensively, especially in scenarios involving different and complex crystal interfaces. This enables precise exploration of light transmission in detector designs where multiple materials are coupled together, addressing the challenges often associated with measuring light sharing in such complex configurations. Indeed, the model we developed can be easily modified to model a very large variety of crystal-coupling-reflector configurations, which can be adapted to the specific characteristics of a radiation detector. Not only the crystal surface and its optical properties can be chosen; the coupling medium characteristics can be customized, together with the one of the reflector. If the reflector reflectance and angular distribution of reflectance are available (both from a producer datasheet or after a benchtop characterization), a large variety of reflectors could be modeled using the LUT model. For example, with the goal of reducing the intercrystal crosstalk, any reflector that shows a high transmittance could be modeled and used to study specific configurations. Examples are specular (ESR coupled with air or grease) or diffusive reflectors (PTFE as Teflon or glossy tape, white titanium dioxide), white reflectors (EJ510), retroreflectors, $BaSO_4$, Lumirror, and Tyvek paper [20], [21], [22]. A natural application of such model is simulating the crosstalk in pixelated detectors where the spatial resolution and energy resolution can be affected by the crosstalk, especially in arrays with the small crystal cross section.

We used two photodetectors, one at the top and one at the bottom of the crystals. Although not a conventional detector configuration (as using two SiPMs on the same crystal side), it appeared to be the optimal configuration to optically decouple the response of the two SiPMs and thus avoid light leakage at the crystal-photodetectors interface.

The experimental measurements were conducted at the low SiPM overvoltage to minimize nuisance contributions from the SiPM crosstalk. By increasing the SiPM overvoltage to +4 or +6 V above the breakdown voltage, we observed an increase in the calculated experimental crystal crosstalk ratio (e.g., 17.1% at +2 V, 18.5% at +4 V, and 20.2% at +6 V for 10 mm thick crystals with the air interface). The reason for this increase arose from unequally distributed external SiPM crosstalk, which was partly transferred to the other SiPM: assuming the gamma-ray interacted in crystal 1, the majority of light was detected by SiPM 1. This means SiPM 1 also emitted a high number of infrared photons [23], which could be detected by SiPM 2. On the other hand, for SiPM 2, only a small amount of light was detected from the initial gamma-ray interaction (since the light needed to be transmitted from crystals 1 to 2). Thus, the generation of photons from the SiPM crosstalk was smaller. Therefore, SiPM 2 detected more secondary photons from SiPM 1 compared to the opposite configuration, which explained the ratio increase with higher SiPM overvoltage. The presented study aimed to understand the intercrystal optical photon crosstalk isolated from other contributions. However, studying the role of SiPMs (e.g., in an array configuration at optimized bias voltage for good energy and time resolution) in combination with the intercrystal optical photon crosstalk is beyond the scope of this work.

V. Conclusion

In this work, the accurate model for optical photon transmission in a scintillation detector has been validated against the experiments for the first time, for different crystal thicknesses and interfaces. The model has been integrated within the LUT Davis algorithm, which was already validated to simulate the reflection of optical photons [13]. It allows the modeling of optical photon refraction accurately when using the different crystal interfaces and is available to all users upon request to the authors. Some optimized LUTs will also be made available to users in the next GATE release. ESR coupled with air appeared to be the interface with the lowest percentage of optical crosstalk, thus optimal for reducing optical crosstalk.

These results show the possibility of simulating and investigating optical photon transmission in all detector designs where multiple materials are coupled together, i.e., where optical crosstalk needs to be accurately taken into account (e.g., pixelated crystals).

ACKNOWLEDGMENT

The authors thank Sun Il Kwon and Daehee Lee for their help with the experimental setup. All authors declare that they have no known conflicts of interest in terms of competing financial interests or personal relationships that could have an influence or are relevant to the work reported in this article.

REFERENCES

[1] C. Levin, M. Tornai, S. Cherry, L. MacDonald, and E. Hoffman, "Compton scatter and X-ray crosstalk and the use of very thin intercrystal septa in high-resolution PET detectors," *IEEE Trans. Nuclear Sci.*, vol. 44, no. 2, pp. 218–224, Apr. 1997. [Online]. Available: https://ieeexplore.ieee.org/abstract/document/568809

[2] P. Vaska, S. Stoll, C. Woody, D. Schlyer, and S. Shokouhi, "Effects of intercrystal crosstalk on multielement LSO/APD PET detectors," *IEEE Trans. Nuclear Sci.*, vol. 50, no. 3, pp. 362–366, Jun. 2003. [Online]. Available: https://ieeexplore.ieee.org/abstract/document/1208595

[3] J. R. Stickel and S. R. Cherry, "High-resolution PET detector design: Modelling components of intrinsic spatial resolution," *Phys. Med. Biol.*, vol. 50, no. 2, pp. 179–195, 2004. [Online]. Available: https://iopscience.iop.org/article/10.1088/0031-9155/50/2/001

[4] C. Degenhardt, K. Fiedler, T. Frach, W. Rutten, T. Solf, and A. Thon, "Impact of Intercrystal crosstalk on depth-of-interaction information in PET detectors," *IEEE Trans. Nuclear Sci.*, vol. 54, no. 3, pp. 427–432, Jun. 2007. [Online]. Available: https://ieeexplore.ieee.org/abstract/document/4237404

[5] N. Kießling, A. Bieberle, and U. Hampel, "Analysis of scattered radiation cross-talk in a high-resolution gamma ray tomography detector with GATE monte-carlo simulation," *Nuclear Instrum. Methods Phys. Res. Sect. A*, vol. 595, no. 2, pp. 375–380, 2008. [Online]. Available: https://www.sciencedirect.com/science/article/pii/S0168900208009200

[6] M. Sakai et al., "Crosstalk reduction using a dual energy window scatter correction in compton imaging," *Sensors*, vol. 20, no. 9, p. 2453, 2020. [Online]. Available: https://www.ncbi.nlm.nih.gov/pmc/articles/PMC7249665/

[7] E. Yoshida, F. Obata, and T. Yamaya, "Simultaneous time-skew and time-walk correction for TOF-PET detector," *Nuclear Instrum. Methods Phys. Res. Sect. A*, vol. 1049, Apr. 2023, Art. no. 168114, doi: 10.1016/j.nima.2023.168114. [Online]. Available: https://www.sciencedirect.com/science/article/pii/S0168900223001043

[8] P. Bebié, W. Lustermann, C. Ritzer, R. Wixinger, and G. Dissertori, "Effects of inter-crystal optical separation layers on unwanted light crosstalk and on performance parameters of the SAFIR PET/MR scanner," in *Proc. IEEE NSS/MIC*, 2021, pp. 1–2.

[9] C. Ritzer et al., "Initial characterization of the SAFIR prototype PET-MR scanner," vol. 4, no. 5, pp. 613–621, Sep. 2020. [Online]. Available: https://ieeexplore.ieee.org/document/9040649

[10] C. Trigila, E. Moghe, and E. Roncali, "Technical note: Standalone application to generate custom reflectance look-up table for advanced optical monte carlo simulation in GATE/Geant4," *Med. Phys.*, vol. 48, no. 6, pp. 2800–2808, 2021. [Online]. Available: https://onlinelibrary.wiley.com/doi/10.1002/mp.14863

[11] D. Sarrut et al., "Advanced monte carlo simulations of emission tomography imaging systems with GATE," *Phys. Med. Biol.*, vol. 66, no. 10, 2021, Art. no. 10TR03. [Online]. Available: https://dx.doi.org/10.1088/1361-6560/abf276

[12] M. Stockhoff, S. Jan, A. Dubois, S. R. Cherry, and E. Roncali, "Advanced optical simulation of scintillation detectors in GATE V8.0: First implementation of a reflectance model based on measured data," *Phys. Med. Biol.*, vol. 62, no. 12, pp. L1–L8, 2017. [Online]. Available: https://iopscience.iop.org/article/10.1088/1361-6560/aa7007

[13] E. Roncali, M. Stockhoff, and S. R. Cherry, "An integrated model of scintillator-reflector properties for advanced simulations of optical transport," *Phys. Med. Biol.*, vol. 62, no. 12, pp. 4811–4830, 2017. [Online]. Available: https://iopscience.iop.org/article/10.1088/1361-6560/aa6ca5

[14] C. Trigila and E. Roncali, "Optimization of scintillator-reflector optical interfaces for the LUT davis model," *Med. Phys.*, vol. 48, no. 9, 2021, Art. no. mp.15109. [Online]. Available: https://onlinelibrary.wiley.com/doi/10.1002/mp.15109

[15] D. J. J. van der Laan, D. R. Schaart, M. C. Maas, F. J. Beekman, P. Bruyndonckx, and C. W. E. van Eijk, "Optical simulation of monolithic scintillator detectors using GATE/GEANT4," *Phys. Med. Biol.*, vol. 55, no. 6, pp. 1659–1675, 2010. [Online]. Available: https://iopscience.iop.org/article/10.1088/0031-9155/55/6/009

[16] "Low breakdown voltage type MPPC for scintillation detector," Datasheet MPPC s14160/s14161, Hamamatsu Photon., Shizuoka, Japan, 2020. [Online]. Available: https://www.hamamatsu.com/content/dam/hamamatsu-photonics/sites/documents/99_SALES_LIBRARY/ssd/s14160_s14161_series_kapd1064e.pdf

[17] N. Kratochwil, S. Gundacker, and E. Auffray, "A roadmap for sole cherenkov radiators with SiPMs in TOF-PET," *Phys. Med. Biol.*, vol. 66, no. 19, 2021, Art. no. 195001. [Online]. Available: https://iopscience.iop.org/article/10.1088/1361-6560/ac212a/meta

[18] J. Pulko, F. R. Schneider, A. Velroyen, D. Renker, and S. I. Ziegler, "A monte-carlo model of a SiPM coupled to a scintillating crystal," *J. Instrum.*, vol. 7, no. 2, 2012, Art. no. P02009. [Online]. Available: https://dx.doi.org/10.1088/1748-0221/7/02/P02009

[19] F. Loignon-Houle, C. Pepin, S. Charlebois, and R. Lecomte, "Reflectivity quenching of ESR multilayer polymer film reflector in optically bonded scintillator arrays," *Nuclear Instrum. Methods Phys. Res. Sect. A*, vol. 851, pp. 62–67, Apr. 2017.

[20] M. Janecek and W. W. Moses, "Optical reflectance measurements for commonly used reflectors," *IEEE Trans. Nuclear Sci.*, vol. 55, no. 4, pp. 2432–2437, Aug. 2008. [Online]. Available: http://ieeexplore.ieee.org/document/4636942/

[21] M. Janecek and W. W. Moses, "Simulating scintillator light collection using measured optical reflectance," *IEEE Trans. Nuclear Sci.*, vol. 57, no. 3, pp. 964–970, Jun. 2010. [Online]. Available: http://ieeexplore.ieee.org/document/5485130/

[22] M. Janecek, "Reflectivity spectra for commonly used reflectors," *IEEE Trans. Nuclear Sci.*, vol. 59, no. 3, pp. 490–497, Jun. 2012. [Online]. Available: http://ieeexplore.ieee.org/document/6168236/

[23] A. Nepomuk Otte, "On the efficiency of photon emission during electrical breakdown in silicon," *Nuclear Instrum. Methods Phys. Res. Sect. A*, vol. 610, no. 1, pp. 105–109, 2009. [Online]. Available: https://www.sciencedirect.com/science/article/pii/S0168900209010390